

Generalized Octet Rule with Fractional Occupancies for Boron

Shaogang Xu,^{II} Changchun He,^{II} Yujun Zhao, Xiaobao Yang, and Hu Xu^{*}



Cite This: *J. Am. Chem. Soc.* 2023, 145, 25003–25009



Read Online

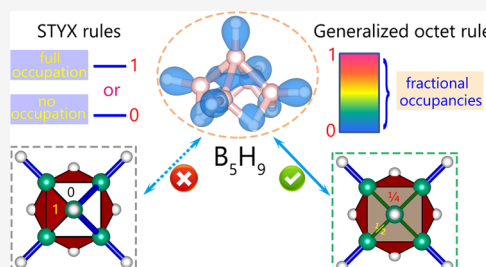
ACCESS |

Metrics & More

Article Recommendations

Supporting Information

ABSTRACT: The octet rule is a fundamental theory in the chemical bonding of main-group elements, which achieve stable configurations by gaining, losing, or sharing electrons. However, the conventional octet rule, as depicted through Lewis structures, is inadequate for describing the electron delocalization in boron allotropes and boron-rich compounds due to the electron deficiency of boron. To address this, we introduce the concept of fractional electron occupancies, which more accurately reflect the electron delocalization in boron systems. Based on this, we propose a generalized octet rule that provides a more comprehensive understanding of the complex bonding configurations in boron allotropes and boron-rich compounds. Importantly, our predictions for $\alpha\text{-B}_{12}$ are validated by both first-principles calculations and existing experimental data. Beyond boron, this generalized octet rule is also applicable to systems with multiple resonance structures.



INTRODUCTION

Chemical bonding models serve as powerful theoretical frameworks for understanding atomic interactions, molecular geometries, and reactivity.¹ Over the past century, various models have emerged, with the foundational work of Lewis and Langmuir in the early 20th century setting the stage for valence bond theory. Lewis introduced the shared electron-pair bonding model,² which Langmuir later expanded upon, introducing terms including covalence and the octet rule.^{3–6} This rule remains a cornerstone for interpreting chemical bonding and molecular properties today.

The octet rule posits that main-group elements form bonds to complete their valence shell with eight electrons, thereby stabilizing their energy levels. The octet rule provides a general basis for describing molecular structures by gaining, losing, or sharing electrons.⁷ As shown in Figure 1, the Lewis electron dot diagrams indicate that the four elements (X = C, N, O, and F) in the second period can realize the full valence shell ($2s^22p^6$) such as neon (Ne) by bonding with hydrogen (H) atoms.

Located between metals and nonmetals, boron (B) is one of the most fascinating elements in the periodic table, which is known for its electron deficiency, complicated bonding configurations, and numerous borides with various properties.⁸ Until now, the polymorphic boron allotropes with different dimensions have been reported, including the crystalline boron in various forms, flexible boron clusters, and various boron sheets composed of triangular and hexagonal vacancies.^{9–11} The polymorphism of boron allotropes is derived from the special bonding configurations among boron atoms.^{8,9,12,13} Furthermore, the structural flexibility of boron allotropes induces a variety of properties, which have been confirmed by recent experimental observations and theoretical calcula-

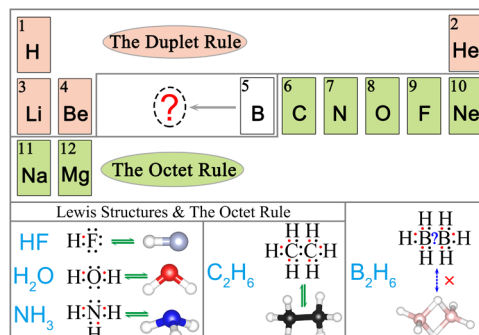


Figure 1. (Upper panel) Periodic table highlighting main-group elements with atomic numbers ranging from 1 to 12. (Lower panel) Lewis structures of selected molecules and the B–H–B bridge bonds in diborane.

tions.^{14–25} Beyond the structural diversity stemming from boron's electron deficiency and vacant p-orbital, boron reagents frequently function as Lewis acids, accepting electrons from donor molecules.²⁶ Notably, the boron-containing frustrated Lewis pairs (FLPs)^{27,28} have emerged as significant players in the advancement of eco-friendly, metal-free catalysis, which have been proved to serve as active sites for N_2 reduction.^{29,30}

Received: September 20, 2023

Revised: October 26, 2023

Accepted: October 26, 2023

Published: November 6, 2023



The peculiarity of boron is an old story, which starts from the borane molecules. It is generally considered that the octet rule in Lewis structures fails to describe the valence electrons in borane molecules due to the electron deficiency of boron. As shown in Figure 1, the unusual B–H–B bridge bond confirmed by the infrared spectra in diborane B_2H_6 cannot be explained by the conventional octet rule based on the two-center two-electron (2c–2e) bond.^{31,32} Instead, a three-center two-electron (3c–2e) bond was proposed to describe the B–H–B bond.³³ Subsequently, because many higher boranes with more complicated structures have been elucidated using X-ray diffraction techniques, Lipscomb et al.³⁴ proposed the famous STYX rules based on 2c–2e and 3c–2e bonds to describe the balance of orbital, hydrogen, and valence electrons in boranes. In addition, Wade's rule³⁵ states that there are $2n + 2$ electrons for the framework of the special *closo* boranes with n vertices. However, the above-mentioned rules are used only to classify certain kinds of bonds in boranes, which cannot explain the bond distributions for a given structure. Furthermore, the STYX and Wade's rules only consider the full occupation of electrons for all the 2c–2e and 3c–2e bonds, while they fall short in explaining bond distributions and electron delocalization in boron systems.

To address these gaps, we introduce a generalized octet rule (GOR) based on well-established 2c–2e and 3c–2e bonding models in boranes. The GOR operates under two constraints to yield unique solutions with fractional electron occupancies for boron-based systems. Our predictions align closely with charge distributions obtained from first-principles calculations and are validated by experimental data for α - B_{12} . Beyond boron, the GOR also accurately describes systems with multiple resonance structures, offering a robust strategy for understanding complex local coordination environments.

METHODS

Structural relaxations were carried out using the Vienna Ab initio Simulation Package (VASP)³⁶ with the electron–ion interactions modeled through the projector augmented wave (PAW) method.³⁷ The exchange-correlation potential was addressed within the framework of the generalized gradient approximation (GGA), employing the Perdew–Burke–Ernzerhof (PBE) functional.³⁸ All atomic positions were fully relaxed until the forces on each atom were reduced to less than 0.01 eV/Å. To achieve more accurate ground-state electron densities, a finer FFT grid was utilized, and the convergence criterion for self-consistent calculations was set to 1×10^{-6} eV per atom. The charge difference for a given structure, $\Delta(\rho)$, is calculated as $\rho(A) - \rho(B)$, where $\rho(A)$ represents the charge densities obtained from self-consistent calculations and $\rho(B)$ is the sum of the charge densities of isolated atoms. Visualization of the charge density difference was accomplished using VESTA software.³⁹

RESULTS AND DISCUSSION

The unique properties of 2p elements can be attributed to the primogenic effect,⁴⁰ which results in radially nodeless 2p valence atomic orbitals that are significantly smaller than their counterparts with main quantum number $n > 2$. This effect leads to pronounced sp-hybrid bonding in light p-block elements, as the 2p subshell has a radial extent similar to that of the 2s subshell. In contrast, heavier p-block elements with $n \geq 3$ exhibit a significant difference between $r(ns)$ and $r(np)$, ranging from approximately –20 to –30%.⁴¹ As a result, the octet rule is generally applicable to elements with $n = 2$, while the 18-electron and 32-electron rules are more relevant for elements with $n > 2$.

For 2p elements including boron, four sp^3 hybrid orbitals are formed by mixing one s and three p orbitals. Given boron's three valence electrons, two half-filled sp^3 hybrid orbitals can bond with two terminal hydrogen atoms in diborane, leaving the remaining two hybrid orbitals for bridging hydrogen atoms. To account for the electron deficiency in boron hydrides, the unique three-center two-electron (3c–2e) bond should be involved. Lipscomb et al.⁴² classified two 2c–2e bonds and three 3c–2e bonds (see Figure 2) and developed the STYX

STYX code for the Boranes (B_nH_{n+m})																												
① Three centers orbital balance : $n = S + T$ ② The hydrogen balance : $m = S + X$ ③ The electron balance : $n + (m/2) = S + T + Y + X$																												
$Y = (S - X)/2; m/2 \leq S \leq m$																												
<table border="1"> <thead> <tr> <th>S</th><th>T</th><th>Y</th><th>X</th></tr> </thead> <tbody> <tr><td>2</td><td>0</td><td>0</td><td>2</td></tr> <tr><td>3</td><td>-1</td><td>1</td><td>1</td></tr> <tr><td>4</td><td>-2</td><td>2</td><td>0</td></tr> </tbody> </table> $B_2H_6 \quad (n = 2, m = 4)$					S	T	Y	X	2	0	0	2	3	-1	1	1	4	-2	2	0								
S	T	Y	X																									
2	0	0	2																									
3	-1	1	1																									
4	-2	2	0																									
<table border="1"> <thead> <tr> <th>S</th><th>T</th><th>Y</th><th>X</th></tr> </thead> <tbody> <tr><td>3</td><td>1</td><td>0</td><td>3</td></tr> <tr><td>4</td><td>0</td><td>1</td><td>2</td></tr> <tr><td>5</td><td>-1</td><td>2</td><td>1</td></tr> <tr><td>6</td><td>-2</td><td>3</td><td>0</td></tr> </tbody> </table> $B_4H_{10} \quad (n = 4, m = 6)$					S	T	Y	X	3	1	0	3	4	0	1	2	5	-1	2	1	6	-2	3	0				
S	T	Y	X																									
3	1	0	3																									
4	0	1	2																									
5	-1	2	1																									
6	-2	3	0																									
<table border="1"> <thead> <tr> <th>S</th><th>T</th><th>Y</th><th>X</th></tr> </thead> <tbody> <tr><td>2</td><td>3</td><td>0</td><td>2</td></tr> <tr><td>3</td><td>2</td><td>1</td><td>1</td></tr> <tr><td>4</td><td>1</td><td>2</td><td>0</td></tr> <tr><td>5</td><td>0</td><td>2</td><td>1</td></tr> <tr><td>6</td><td>-1</td><td>3</td><td>0</td></tr> </tbody> </table> $B_5H_9 \quad (n = 5, m = 4)$					S	T	Y	X	2	3	0	2	3	2	1	1	4	1	2	0	5	0	2	1	6	-1	3	0
S	T	Y	X																									
2	3	0	2																									
3	2	1	1																									
4	1	2	0																									
5	0	2	1																									
6	-1	3	0																									
<table border="1"> <thead> <tr> <th>S</th><th>T</th><th>Y</th><th>X</th></tr> </thead> <tbody> <tr><td>3</td><td>2</td><td>0</td><td>3</td></tr> <tr><td>4</td><td>1</td><td>1</td><td>2</td></tr> <tr><td>5</td><td>0</td><td>2</td><td>1</td></tr> <tr><td>6</td><td>-1</td><td>3</td><td>0</td></tr> </tbody> </table> $B_5H_{11} \quad (n = 5, m = 6)$					S	T	Y	X	3	2	0	3	4	1	1	2	5	0	2	1	6	-1	3	0				
S	T	Y	X																									
3	2	0	3																									
4	1	1	2																									
5	0	2	1																									
6	-1	3	0																									

Figure 2. (Left panel) Five distinct bond types found in borane structures. (Right panel) Key components of the STYX rules and potential STYX number sets for given boranes. Note: sets in the shaded areas represent invalid solutions with negative values.

rules to balance atoms, orbitals, and electrons in neutral boranes. In these rules, S, T, Y, and X denote the number of B–H–B bonds, the number of B–B–B bonds, the number of B–B bonds, and the number of BH_2 groups, respectively. These rules remain a standard tool for analyzing neutral boranes and are included in current inorganic chemistry textbooks.⁴³ However, the STYX rules have limitations; they can yield multiple possible sets of STYX numbers for a given borane formula, and the same STYX code may correspond to different structural topologies.

In this work, we introduce a generalized octet rule (GOR) with fractional occupancies to describe the bond distributions in boron allotropes and boron-rich compounds. We assume that the 3c–2e bonds are located in the B–B–B/B–H–B triangular regions and that the B–B/B–H single bonds are traditional 2c–2e bonds. The GOR employs two key constraints: (1) an 8-electron rule based on the nearest-neighbor bonding distributions for each boron atom and (2) a constraint ensuring that the total number of valence electrons equals the sum of all 2c–2e and 3c–2e bonds. These constraints allow us to formulate linear equations and solve for fractional occupation numbers, confined to the range of [0, 1]. This approach aligns with valence bond (VB) theory, where the actual electron distribution is a superposition of various Lewis structures. Thus, the fractional occupations arise naturally in this framework as a result of averaging over multiple resonance forms, which can be deduced from the view of quantum mechanics (see the Supporting Information for details).

We first apply the GOR to B_2H_6 and B_4H_{10} , obtaining unique bond distributions that align with the calculated charge

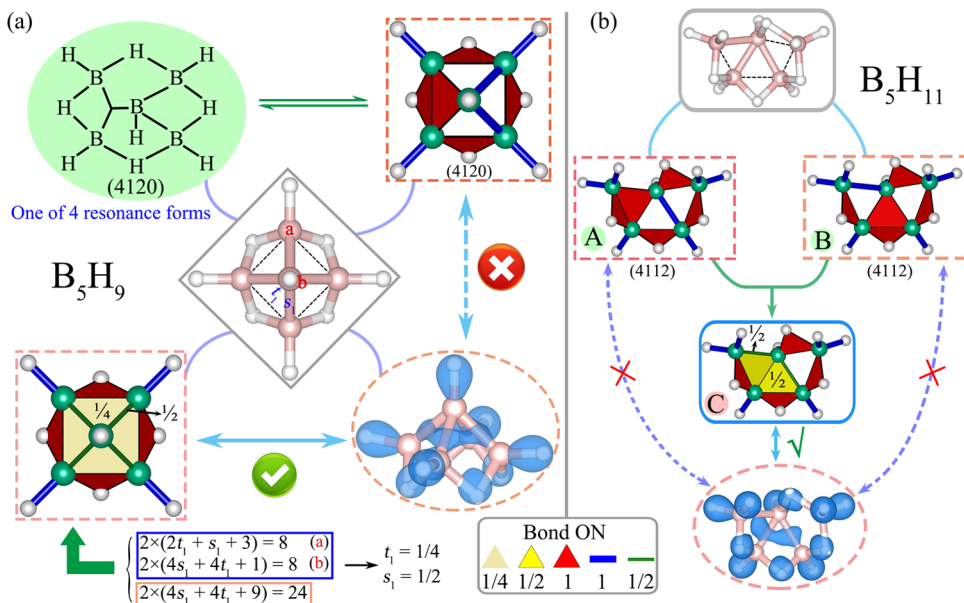


Figure 3. (a) One of the four resonance structures, charge density difference, and model analysis for B_5H_9 . (b) Three sets of bond distributions and the corresponding charge density difference for B_5H_{11} . Note: the isovalue is set at $0.02 \text{ e}/\text{bohr}^{-3}$ and bond occupation numbers (ON) are displayed in the center of the figure.

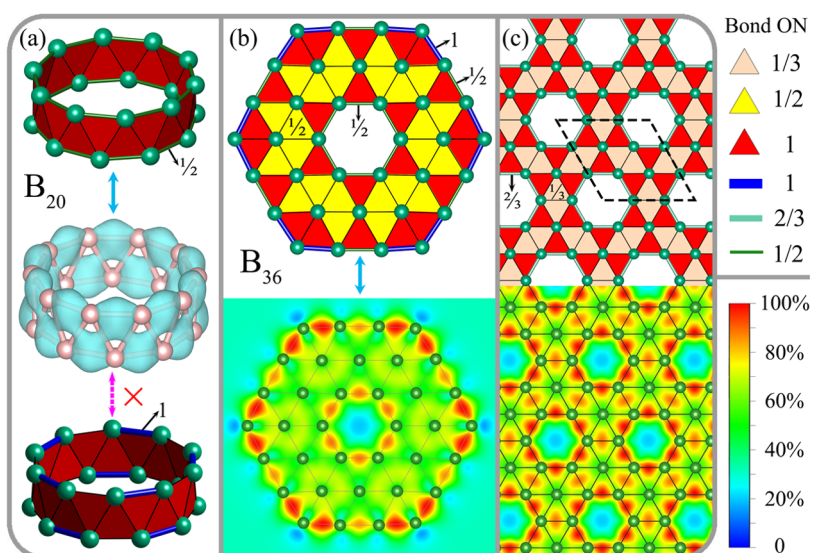


Figure 4. (a) Two sets of bond distributions along with charge density difference for the B_{20} cluster. (b) Bond distributions featuring fractional occupancies and planar charge difference for the B_{36} cluster. (c) Bond distributions with fractional occupancies and planar charge difference for the α -sheet. Note: The isovalue for B_{20} is $0.02 \text{ e}/\text{bohr}^{-3}$. Bond occupation numbers (ON) and color bar percentages for the isosurfaces in parts (b, c) are listed on the right side of the figure.

density differences, as shown in Figure S1. With the increase in boron atoms, the geometries of higher borane molecules become more complicated, and the delocalized electrons in the higher boranes can be explained by the following analysis. For a neutral borane (B_nH_{n+m}) molecule, the total number of electron pairs is $2n + m/2$. Considering the duplet rule of the H atom, the number of electron pairs shared by B–H and B–H–B local motifs is $n + m$ and the number of remaining electron pairs belonging to B–B/B–B–B regions is $\kappa = n - m/2$. Then, we can confirm κ for a given borane, and κ for a higher borane with $n > 4$ is greater than 1, as shown in Table S1. Clearly, the total valence electrons in the higher boranes with $n \geq 4$ can not only be consumed by the B–H and B–H–

B parts, which results in more remaining electrons for the regions of boron. Therefore, the electron delocalization effect must be considered.

For pentaborane (B_5H_9), there are five B atoms arranged in a square pyramid. Each B has a terminal hydride ligand, and four hydrides span the four edges of the pyramid (Figure 3(a)). Considering the C_{4v} symmetry of B_5H_9 , the planar view in Figure 3(a) analyzed by the STYX rules is one of the 4 equiv resonance forms, which cannot match with the actual charge density difference. By analyzing the geometry of B_5H_9 , we identify two inequivalent B atoms (a, b) and two inequivalent bonds (t_1, s_1). By adopting the workflow of the GOR, we construct the linear equations for B_5H_9 , and the unique

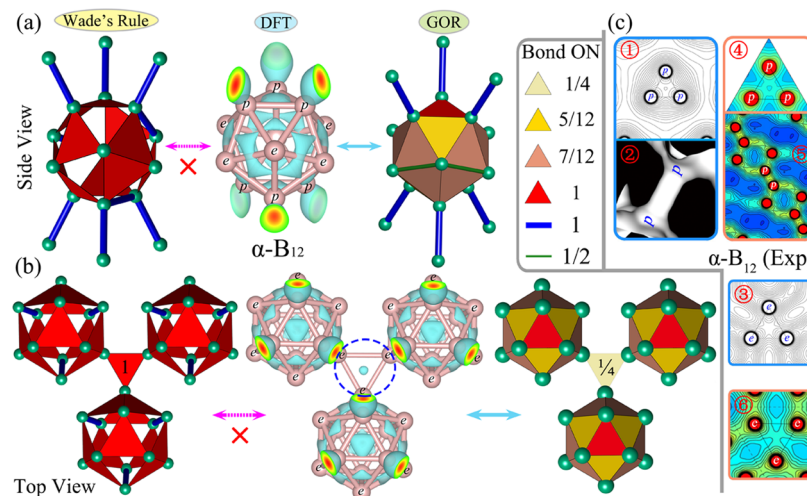


Figure 5. (a, b) Bond distributions and charge density difference for $\alpha\text{-B}_{12}$. (c) Experimentally determined electron density distributions for $\alpha\text{-B}_{12}$. Panels (1–3) show the multipole electron density, reprinted with permission from ref 57, Copyright 2013 by American Physical Society. Panels (4–6) show MEM electron density, reprinted with permission from ref 58, Copyright 2015 by Elsevier Masson SAS. Note: The two inequivalent crystallographic sites in $\alpha\text{-B}_{12}$ are labeled as polar (p) and equatorial (e). The isovalue for $\alpha\text{-B}_{12}$ is set at 0.02 e/bohr⁻³, and bond occupation numbers (ON) are displayed in the center of the figure.

solution set ($s_1 = 1/2$, $t_1 = 1/4$) can be deduced. Furthermore, the planar view of (4120) can be represented through a three-dimensional (3D) bond distribution, and the solution with fractional occupancies ($s_1 = 1/2$, $t_1 = 1/4$) can be seen as the statistical average of the four equivalent resonance structures. Clearly, the charge density difference of B_5H_9 also shows C_{4v} symmetry, which can be described by the results with fractional occupancies. Different from the high symmetry of B_5H_9 , the B_5H_{11} molecule is asymmetrical, and we can find two inequivalent resonance bond distributions (A, B) based on the STYX rules (see Figure 3(b)). Although there is an evident mismatch between A and B in charge distributions, their average value (C) with fractional occupancies can satisfy the calculated charge distributions. Similarly, further examples of higher boranes with more complicated structures can be reasonably explained by the GOR, as shown in Figure S2. Compared with the analysis based on the STYX rules, our results with fractional occupancies accurately reflect the delocalized electrons in the pure boron regions. The charge distribution in common carboranes with polyhedral structures can be understood by the GOR (see Figure S3). In addition, for the tetrahedral and octahedral $\text{B}_n\text{H}_n^{0/2-}$ clusters,⁴⁴ we can also apply the GOR to understand the corresponding bonding patterns (see Figure S4).

Our results validate the presence of fractional occupancies in boron-rich regions within boranes. Beyond elucidating chemical bonding, the GOR also offers insights into structural stability under its two governing constraints (see the Supporting Information for details). For instance, the structural transformation of B_4H_x molecules is well accounted for by the GOR (see Figure S5). In the following, the complicated bonding situations in pure boron allotropes are examined. The highly diverse bonding patterns in boron clusters have long been a subject of debate, especially given the increasing variety of isomers as a function of size.⁹

The B_{20} neutral cluster serves as the first transition from planar to tubular boron nanostructures and is considered the precursor to the thinnest boron nanotubes.⁴⁵ The planar B_{36} cluster (the first time borophene was proposed) is a highly

stable structure with perfect C_{6v} hexagonal symmetry, serving as a potential building block for extended boron monolayers.⁴⁶ For B_{20} and B_{36} , considering only full (1) or empty (0) occupation numbers yields resonance bond distributions (see the lower panel of Figures 4(a) and S6a). However, due to the rotational symmetry in B_{20} , a unique fractional occupancy solution ($s_i = 1/2$) emerges for its peripheral 2c–2e bonds, aligning well with the isosurface charge density difference (see the upper panel of Figure 4(a)). For the B_{36} cluster, due to the low coordination number (CN) of B atoms at the edges, the planar charge difference indicates the charge localization at the vertexes of the profile, and the charge distributions in the vicinity of the B atoms with CN = 6 are relatively uniform. Although the two resonance forms of B_{36} satisfy its sixfold symmetry, the bond distributions with 0 and 1 fail to describe the delocalized electrons of the inner B–B–B triangles (see Figure S6a). On the contrary, the model solution with fractional occupations of 1/2 is more reasonable, serving as an average of the two resonance forms (see Figure 4(b)). Similarly, the B_{40} (borospherene)⁴⁷ and tubular B_{42} clusters⁴⁸ can also be understood by the GOR with fractional occupancies (see Figure S6 for details). Therefore, the GOR provides a clear and simple picture for understanding the complicated charge distributions in stable boron clusters. Beyond these intricate local bonding environments, the aromaticity of boron-based clusters remains a pivotal subject within boron chemistry.^{49–51} By introducing the concept of fractional numbers of electrons, the GOR can accurately describe the delocalized electrons in boron-rich materials, with electron delocalization standing as a hallmark of aromatic compounds. Although the GOR does not differentiate between π -bonds and σ -bonds, it serves as an auxiliary tool for qualitatively inferring the aromaticity of borides.

Compared with the boron clusters, boron monolayers have garnered considerable attention for their polymorphism, both in theoretical studies and experimental work.¹⁰ Unlike boranes, the variables (s_i , t_j) in periodic boron systems should satisfy translational symmetry. As the most representative boron monolayer, α -sheet is the first predicted monolayer with D_{6h}

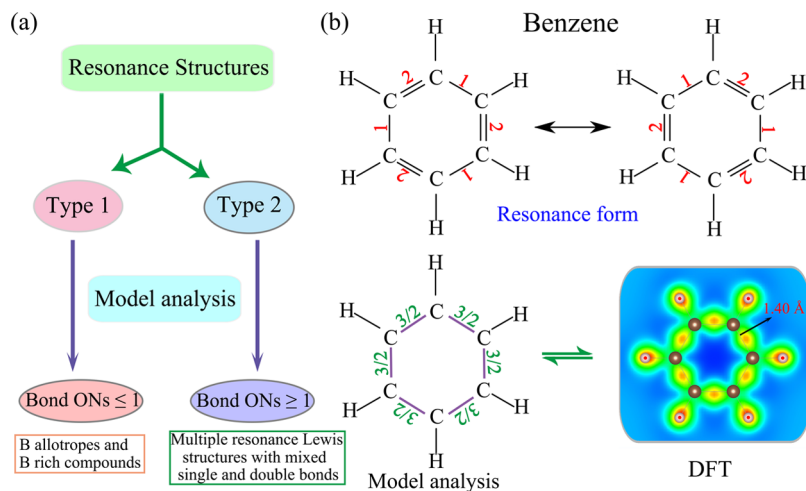


Figure 6. (a) Classification of systems described by multiple resonance structures into two types. (b) Two resonance forms and our model analysis for the benzene molecule.

symmetry,^{52,53} which can be derived from an unfolded B_{80} fullerene.⁵⁴ As shown in Figure 4(c), all the hexagonal edges in the α -sheet are equivalent, and we derive a unique solution with fractional occupancies for the hexagonal edges and the inner triangles, which reveals the relative intensity of the local charge distributions. Moreover, the stable boron bilayers and boron carbide monolayers can also be understood through the GOR framework (Figure S7).

Turning to crystalline boron, its complex chemistry has long been a subject of debate,⁸ particularly the charge distribution in the α -rhombohedral phase (α - B_{12}). Advanced experimental techniques, such as the maximum entropy method (MEM)^{55–58} with powder diffraction data, have provided insights into the electron density distribution in α - B_{12} . These studies highlight the strong charge localization in intraicosahedral (p–p–p) 3c–2e bonds and the relative weakness of intericosahedral (e–e–e) bonds (see Figure 5(c)). The bond distributions in α - B_{12} are usually explained by Wade's rule, which allocates 26 valence electrons to intraicosahedral bonds and 10 to intericosahedral bonds. As shown in the left panels of Figure 5(a,b), the intraicosahedral bonds include ten B–B–B 3c–2e bonds and three B–B 2c–2e bonds, and the intericosahedral bonds include six shared 2c–2e bonds with the icosahedra of neighboring layers and six shared e–e–e 3c–2e bonds with the neighboring icosahedra in the same layer. Clearly, the significant difference in experimental measurements between p–p–p and e–e–e 3c–2e bonds in Figure 5(c) cannot be understood by the analysis based on Wade's rule because Wade's rule assigns identical occupation numbers to all bonds. In addition, Wade's rule ignores the symmetry of intraicosahedral bonds, a feature that is inconsistent with our calculated charge density differences (middle panel of Figure 5(a)).

We extend our GOR analysis to α - B_{12} , obtaining a solution set with fractional occupancies that aligns well with experimental observations^{55–58} and first-principles calculations (see the right panels of Figure 5(a,b)). The strong intraicosahedral p–p–p bonds, highlighted by their high electron density, and weaker intericosahedral e–e–e bonds are both accurately captured by our GOR model. Importantly, the GOR naturally incorporates the symmetry of α - B_{12} and reflects the electron delocalization effect, making it a versatile tool for

understanding a wide range of boron-rich solids formed by linked polyhedra.

The applicability of the GOR extends beyond boron to systems with multiple resonance structures. Based on the fractional occupation numbers (ONs) derived from the GOR, resonance structures can be categorized into two types: (1) those with derived bond ONs smaller than 1, relevant for electron-deficient systems like boron-rich materials, and (2) those with derived bond ONs greater than 1, such as systems represented by multiple Lewis structures with mixed single and double bonds. For instance, benzene has two contributing resonance structures where single and double bonds interchange (Figure 6(b)). While the bond lengths of a C–C single bond and a C=C double bond are 1.47 and 1.35 Å, respectively, all carbon–carbon bonds in benzene measure approximately 1.40 Å.⁵⁹ By applying the 8-electron constraint to the carbon atoms in benzene, we deduce an occupation number of 3/2 for the six equivalent carbon–carbon bonds. This is consistent with abundant experimental data, which show that the real molecule exists as a unique structure rather than any one of the contributing resonance forms. Therefore, the GOR provides an enhanced understanding of systems with multiple resonance structures, including graphene and other molecular/ion species, as elaborated in the Supporting Information. Regarding the multiple resonance structures of metallacycles, incorporating an 18- or 32-electron constraint becomes essential to accurately describe the complex local coordination environments surrounding the central transition metal atom. This expansion of the GOR merits comprehensive investigation in future studies.

CONCLUSIONS

In summary, we have introduced a generalized octet rule (GOR) featuring fractional occupancies to describe the complex bonding configurations and charge distributions in boranes and boron allotropes. The GOR successfully resolves discrepancies between actual charge density differences and bond distributions predicted by traditional STYX rules, particularly in higher boranes. Moreover, the GOR offers valuable insights into the intricate coordination environments and vacancy distributions in neutral boron clusters and two-dimensional boron allotropes. Notably, our model yields a consistent set of fractional occupancies for both intra- and

intericosahedral bonds in α -B₁₂, aligning well with existing experimental data and our theoretical calculations. The incorporation of fractional occupancies enhances our understanding of boron chemistry and offers a new avenue for the design of boron-based materials. Beyond boron, the GOR serves as a reliable tool for capturing local bonding distributions, thereby enriching our understanding of both molecular and solid-state structures.

■ ASSOCIATED CONTENT

§ Supporting Information

The Supporting Information is available free of charge at <https://pubs.acs.org/doi/10.1021/jacs.3c10370>.

Model analysis for various boron-based materials, origin of fractional occupation, and range of applicability and limitation of the GOR ([PDF](#))

■ AUTHOR INFORMATION

Corresponding Author

Hu Xu – Department of Physics, Southern University of Science and Technology, Shenzhen 518055, People's Republic of China; Quantum Science Center of Guangdong-Hong Kong-Macao Greater Bay Area (Guangdong), Shenzhen 518045, People's Republic of China;  orcid.org/0000-0002-2254-5840; Email: xuh@sustech.edu.cn

Authors

Shaogang Xu – Department of Physics, Southern University of Science and Technology, Shenzhen 518055, People's Republic of China; Quantum Science Center of Guangdong-Hong Kong-Macao Greater Bay Area (Guangdong), Shenzhen 518045, People's Republic of China

Changchun He – Department of Physics, South China University of Technology, Guangzhou 510640, People's Republic of China

Yujun Zhao – Department of Physics, South China University of Technology, Guangzhou 510640, People's Republic of China;  orcid.org/0000-0002-6923-1099

Xiaobao Yang – Department of Physics, South China University of Technology, Guangzhou 510640, People's Republic of China;  orcid.org/0000-0001-8851-1988

Complete contact information is available at:

<https://pubs.acs.org/10.1021/jacs.3c10370>

Author Contributions

¶S.X. and C.H. contributed equally to this work.

Notes

The authors declare no competing financial interest.

■ ACKNOWLEDGMENTS

This work was supported by the National Key R&D Program of China (Grant No. 2022YFA1403700), the National Natural Science Foundation of China (Grant Nos. 12374182, 11974160 and 12204224), the Shenzhen Science and Technology Program (Grant No. RCYX20200714114523069), the Guangdong Basic and Applied Basic Research Foundation (Grant No. 2023A1515010734), and the Key-Area Research and Development Program of Guangdong Province (Grant No. 2020B010183001). The computer time at the Center for Computational Science and Engineering at Southern University of Science and Technology is gratefully acknowledged.

■ REFERENCES

- (1) Zhao, L.; Pan, S.; Holzmann, N.; Schwerdtfeger, P.; Frenking, G. Chemical Bonding and Bonding Models of Main-Group Compounds. *Chem. Rev.* **2019**, *119*, 8781–8845.
- (2) Lewis, G. N. The atom and the molecule. *J. Am. Chem. Soc.* **1916**, *38*, 762–785.
- (3) Langmuir, I. The arrangement of electrons in atoms and molecules. *J. Am. Chem. Soc.* **1919**, *41*, 868–934.
- (4) Langmuir, I. Isomorphism, isosterism and covalence. *J. Am. Chem. Soc.* **1919**, *41*, 1543–1559.
- (5) Langmuir, I. The octet theory of valence and its applications with special reference to organic nitrogen compounds. *J. Am. Chem. Soc.* **1920**, *42*, 274–292.
- (6) Langmuir, I. Types of valence. *Science* **1921**, *54*, 59–67.
- (7) Zhao, L.; Schwarz, W. H. E.; Frenking, G. The Lewis electron-pair bonding model: the physical background, one century later. *Nat. Rev. Chem.* **2019**, *3*, 35–47.
- (8) Albert, B.; Hillebrecht, H. Boron: elementary challenge for experimenters and theoreticians. *Angew. Chem., Int. Ed.* **2009**, *48*, 8640–8668.
- (9) Sergeeva, A. P.; Popov, I. A.; Piazza, Z. A.; Li, W.-L.; Romanescu, C.; Wang, L.-S.; Boldyrev, A. I. Understanding boron through size-selected clusters: structure, chemical bonding, and fluxionality. *Acc. Chem. Res.* **2014**, *47*, 1349–1358.
- (10) Zhang, Z.; Penev, E. S.; Yakobson, B. I. Two-dimensional boron: structures, properties and applications. *Chem. Soc. Rev.* **2017**, *46*, 6746–6763.
- (11) Liu, X.; Zhang, Z.; Wang, L.; Yakobson, B. I.; Hersam, M. C. Intermixing and periodic self-assembly of borophene line defects. *Nat. Mater.* **2018**, *17*, 783–788.
- (12) De, S.; Willand, A.; Amsler, M.; Pochet, P.; Genovese, L.; Goedecker, S. Energy Landscape of Fullerene Materials: A Comparison of Boron to Boron Nitride and Carbon. *Phys. Rev. Lett.* **2011**, *106*, No. 225502.
- (13) Deringer, V. L.; Pickard, C. J.; Csányi, G. Data-Driven Learning of Total and Local Energies in Elemental Boron. *Phys. Rev. Lett.* **2018**, *120*, No. 156001.
- (14) Zhou, X.-F.; Dong, X.; Oganov, A. R.; Zhu, Q.; Tian, Y.; Wang, H.-T. Semimetallic Two-Dimensional Boron Allotrope with Massless Dirac Fermions. *Phys. Rev. Lett.* **2014**, *112*, No. 085502.
- (15) Feng, B.; Sugino, O.; Liu, R. Y.; et al. Dirac Fermions in Borophene. *Phys. Rev. Lett.* **2017**, *118*, No. 096401.
- (16) Xu, S.-G.; Li, X.-T.; Zhao, Y.-J.; Liao, J.-H.; Xu, W.-P.; Yang, X.-B.; Xu, H. Two-Dimensional Semiconducting Boron Monolayers. *J. Am. Chem. Soc.* **2017**, *139*, 17233–17236.
- (17) Oganov, A. R.; Chen, J.; Gatti, C.; Ma, Y.; Ma, Y.; Glass, C. W.; Liu, Z.; Yu, T.; Kurakevych, O. O.; Solozhenko, V. L. Ionic high-pressure form of elemental boron. *Nature* **2009**, *457*, 863–867.
- (18) Zhou, X.-F.; Oganov, A. R.; Wang, Z.; Popov, I. A.; Boldyrev, A. I.; Wang, H.-T. Two-dimensional magnetic boron. *Phys. Rev. B* **2016**, *93*, No. 085406.
- (19) Mannix, A. J.; Zhang, Z.; Guisinger, N. P.; Yakobson, B. I.; Hersam, M. C. Borophene as a prototype for synthetic 2D materials development. *Nat. Nanotechnol.* **2018**, *13*, 444–450.
- (20) Xu, S.-G.; Zheng, B.; Xu, H.; Yang, X.-B. Ideal Nodal Line Semimetal in a Two-Dimensional Boron Bilayer. *J. Phys. Chem. C* **2019**, *123*, 4977–4983.
- (21) Zhu, M.-H.; Weng, X.-J.; Gao, G.; Dong, S.; Lin, L.-F.; Wang, W.-H.; Zhu, Q.; Oganov, A. R.; Dong, X.; Tian, Y.; Zhou, X.-F.; Wang, H.-T. Magnetic borophenes from an evolutionary search. *Phys. Rev. B* **2019**, *99*, No. 205412.
- (22) Tkachenko, N. V.; Steglenko, D.; Fedik, N.; Boldyrev, N. M.; Minyaev, R. M.; Minkin, V. I.; Boldyrev, A. I. Superoctahedral two-dimensional metallic boron with peculiar magnetic properties. *Phys. Chem. Chem. Phys.* **2019**, *21*, 19764–19771.
- (23) He, C.-C.; Xu, S.-G.; Zhao, Y.-J.; Xu, H.; Yang, X.-B. All-boron planar ferromagnetic structures: from clusters to monolayers. *Nanoscale* **2021**, *13*, 9881–9887.

- (24) Lian, C.; Hu, S.-Q.; Zhang, J.; Cheng, C.; Yuan, Z.; Gao, S.; Meng, S. Integrated Plasmonics: Broadband Dirac Plasmons in Borophene. *Phys. Rev. Lett.* **2020**, *125*, No. 116802.
- (25) Xu, S.-G.; He, C.-C.; Zhao, Y.-J.; Xu, H.; Yang, X.-B. Unconventional line defects engineering in two-dimensional boron monolayers. *Phys. Rev. Mater.* **2021**, *5*, No. 044003.
- (26) Nori, V.; Pesciaoli, F.; Sinibaldi, A.; Giorgianni, G.; Carloni, A. Boron-based Lewis acid catalysis: Challenges and perspectives. *Catalysts* **2022**, *12*, No. 5.
- (27) McCahill, J. S.; Welch, G. C.; Stephan, D. W. Reactivity of “Frustrated Lewis Pairs”: Three-Component Reactions of Phosphines, a Borane, and Olefins. *Angew. Chem., Int. Ed.* **2007**, *46*, 4968–4971.
- (28) Stephan, D. W. Catalysis, FLPs, and beyond. *Chem* **2020**, *6*, 1520–1526.
- (29) Légaré, M.-A.; Bélanger-Chabot, G.; Dewhurst, R. D.; Welz, E.; Krummenacher, I.; Engels, B.; Braunschweig, H. Nitrogen fixation and reduction at boron. *Science* **2018**, *359*, 896–900.
- (30) Ling, C.; Niu, X.; Li, Q.; Du, A.; Wang, J. Metal-free single atom catalyst for N_2 fixation driven by visible light. *J. Am. Chem. Soc.* **2018**, *140*, 14161–14168.
- (31) Price, W. C. The structure of diborane. *J. Chem. Phys.* **1947**, *15*, 614.
- (32) Hedberg, K.; Schomaker, V. A Reinvestigation of the Structures of Diborane and Ethane by Electron Diffraction^{1,2}. *J. Am. Chem. Soc.* **1951**, *73*, 1482–1487.
- (33) Longuet-Higgins, H. Substances hydrogénées avec défaut d'électrons. *J. Chim. Phys.* **1949**, *46*, 268–275.
- (34) Lipscomb, W. N. The boranes and their relatives. *Science* **1977**, *196*, 1047–1055.
- (35) Jemmis, E. D.; Balakrishnarajan, M. M.; Pancharatna, P. D. A unifying electron-counting rule for macropolyhedral boranes, metalaboranes, and metallocenes. *J. Am. Chem. Soc.* **2001**, *123*, 4313–4323.
- (36) Kresse, G.; Furthmüller, J. Efficient iterative schemes for ab initio total-energy calculations using a plane-wave basis set. *Phys. Rev. B* **1996**, *54*, 11169–11186.
- (37) Kresse, G.; Joubert, D. From ultrasoft pseudopotentials to the projector augmented-wave method. *Phys. Rev. B* **1999**, *59*, 1758–1775.
- (38) Perdew, J. P.; Burke, K.; Ernzerhof, M. Generalized Gradient Approximation Made Simple. *Phys. Rev. Lett.* **1996**, *77*, 3865–3868.
- (39) Momma, K.; Izumi, F. VESTA 3 for three-dimensional visualization of crystal, volumetric and morphology data. *J. Appl. Crystallogr.* **2011**, *44*, 1272–1276.
- (40) Cao, C.-S.; Hu, H.-S.; Li, J.; Schwarz, W. H. E. Physical origin of chemical periodicities in the system of elements. *Pure Appl. Chem.* **2019**, *91*, 1969–1999.
- (41) Wang, Z.-L.; Hu, H.-S.; von Szentpály, L.; Stoll, H.; Fritzsche, S.; Pyykö, P.; Schwarz, W. H. E.; Li, J. Understanding the uniqueness of 2p elements in periodic tables. *Chem. - Eur. J.* **2020**, *26*, 15558–15564.
- (42) Eberhardt, W. H.; Crawford, B., Jr.; Lipscomb, W. N. The valence structure of the boron hydrides. *J. Chem. Phys.* **1954**, *22*, 989–1001.
- (43) Dalal, M. *A Textbook of Inorganic Chemistry-Vol. 1*; Dalal Institute, 2017.
- (44) Wang, R.-Y.; Zhang, J.-X.; Jiang, X.-L.; Ma, N.; Chen, X.; Xu, C.-Q.; Li, J. Understanding the Electronic Structure and Stability of $\text{B}_n\text{X}_n^{0/2-}$ ($n = 4, 6$; $\text{X} = \text{H}, \text{F}, \text{Cl}, \text{Br}, \text{I}, \text{At}, \text{Ts}$) Clusters. *Chin. J. Chem.* **2021**, *39*, 1811–1818.
- (45) Kiran, B.; Bulusu, S.; Zhai, H.-J.; Yoo, S.; Zeng, X. C.; Wang, L.-S. Planar-to-tubular structural transition in boron clusters: B_{20} as the embryo of single-walled boron nanotubes. *Proc. Natl. Acad. Sci. U.S.A.* **2005**, *102*, 961–964.
- (46) Piazza, Z. A.; Hu, H.-S.; Li, W.-L.; Zhao, Y.-F.; Li, J.; Wang, L.-S. Planar hexagonal B_{36} as a potential basis for extended single-atom layer boron sheets. *Nat. Commun.* **2014**, *5*, No. 3113.
- (47) Zhai, H.-J.; Zhao, Y. F.; Li, W. L.; et al. Observation of an all-boron fullerene. *Nat. Chem.* **2014**, *6*, 727–731.
- (48) Bai, H.; Chen, T.-T.; Chen, Q.; Zhao, X.-Y.; Zhang, Y.-Y.; Chen, W.-J.; Li, W.-L.; Cheung, L. F.; Bai, B.; Cavanagh, J.; Huang, W.; Li, S.-D.; Li, J.; Wang, L.-S. Planar B_{41}^- and B_{42}^- clusters with double-hexagonal vacancies. *Nanoscale* **2019**, *11*, 23286–23295.
- (49) Chen, Z.; King, R. B. Spherical aromaticity: recent work on fullerenes, polyhedral boranes, and related structures. *Chem. Rev.* **2005**, *105*, 3613–3642.
- (50) Chen, T.-T.; Cheung, L. F.; Wang, L.-S. Probing the nature of the transition-metal-boron bonds and novel aromaticity in small metal-doped boron clusters using photoelectron spectroscopy. *Annu. Rev. Phys. Chem.* **2022**, *73*, 233–253.
- (51) Poater, J.; Viñas, C.; Bennour, I.; Escayola, S.; Solà, M.; Teixidor, F. Too persistent to give up: Aromaticity in boron clusters survives radical structural changes. *J. Am. Chem. Soc.* **2020**, *142*, 9396–9407.
- (52) Tang, H.; Ismail-Beigi, S. Novel precursors for boron nanotubes: the competition of two-center and three-center bonding in boron sheets. *Phys. Rev. Lett.* **2007**, *99*, No. 115501.
- (53) Yang, X.; Ding, Y.; Ni, J. Ab initio prediction of stable boron sheets and boron nanotubes: structure, stability, and electronic properties. *Phys. Rev. B* **2008**, *77*, No. 041402.
- (54) Gonzalez Szwacki, N.; Sadrzadeh, A.; Yakobson, B. I. B_{80} fullerene: an ab initio prediction of geometry, stability, and electronic structure. *Phys. Rev. Lett.* **2007**, *98*, No. 166804.
- (55) Fujimori, M.; Nakata, T.; Nakayama, T.; Nishibori, E.; Kimura, K.; Takata, M.; Sakata, M. Peculiar covalent bonds in α -rhombohedral boron. *Phys. Rev. Lett.* **1999**, *82*, No. 4452.
- (56) Hosoi, S.; Kim, H.; Nagata, T.; Kirihara, K.; Soga, K.; Kimura, K.; Kato, K.; Takata, M. Electron density distributions in derivative crystals of α -rhombohedral boron. *J. Phys. Soc. Jpn.* **2007**, *76*, No. 044602.
- (57) Mondal, S.; van Smaalen, S.; Parakhonskiy, G.; Prathapa, S. J.; Noohinejad, L.; Bykova, E.; Dubrovinskaya, N.; Chernyshov, D.; Dubrovinsky, L. Experimental evidence of orbital order in $\alpha\text{-B}_{12}$ and $\gamma\text{-B}_{28}$ polymorphs of elemental boron. *Phys. Rev. B* **2013**, *88*, No. 024118.
- (58) Nishibori, E.; Hyodo, H.; Kimura, K.; Takata, M. Revisit: High resolution charge density study of α -rhombohedral boron using third-generation SR data at SPring-8. *Solid State Sci.* **2015**, *47*, 27–31.
- (59) Bacon, G. E.; Curry, N. A.; Wilson, S. A.; Spence, R. A crystallographic study of solid benzene by neutron diffraction. *Proc. R. Soc. London, Ser. A* **1964**, *279*, 98–110.